Excitation of weakly bound Rydberg electrons by half-cycle pulses

O. Zobay[1] and G. Alber[2]
[1]*Optical Sciences Center, University of Arizona, Tucson, Arizona 85721*
[2]*Abteilung für Quantenphysik, Universität Ulm, 89069 Ulm, Germany*
(Received 5 February 1999)

The interaction of a weakly bound Rydberg electron with an electromagnetic half-cycle pulse (HCP) is described with the help of a multidimensional semiclassical treatment. This approach relates the quantum evolution of the electron to its underlying classical dynamics. The method is nonperturbative, and is valid for arbitrary spatial and temporal shapes of the applied HCP. On the basis of this approach, angle- and energy-resolved spectra resulting from the ionization of Rydberg atoms by HCP's are analyzed. The different types of spectra obtainable in the sudden-impact approximation are characterized in terms of the appearing semiclassical scattering phenomena. Typical modifications of the spectra originating from finite-pulse effects are discussed. [S1050-2947(99)03108-X]

PACS number(s): 32.80.Rm, 03.65.Sq

I. INTRODUCTION

Recent experimental [1–3] and theoretical [4–6] investigations have demonstrated that (almost) unipolar, high-power electromagnetic field pulses are a useful new spectroscopic tool which is particularly well suited for investigating the dynamics of weakly bound Rydberg electrons. In current experiments the duration τ of these half-cycle pulses (HCP's) extends from the subpicosecond to the nanosecond regime. Several features distinguish the interaction of Rydberg electrons with this new type of electromagnetic radiation from the interaction with conventional laser light or microwave fields. First of all, and in contrast to the optical case, the HCP interacts with the Rydberg electron at every point of its orbit. Furthermore, due to its unipolar nature the influence of the HCP on the electron can often be described in relatively simple and intuitive terms, e.g., with the help of the so-called sudden-impact approximation where the effect of the HCP is modeled as an instantaneous momentum change. Finally, the energy transfer between an oscillating electromagnetic field and a Rydberg electron is always governed by an approximate energy conservation whose energy uncertainty is typically small in comparison with the amount of energy transferred. As HCP's are almost unipolar, such an approximate energy conservation does not hold, and arbitrary amounts of energies can be transferred to a charged particle from zero up to a maximum amount of the order of $\hbar/\tau$.

These characteristic features give rise to interesting phenomena which have been explored in a number of recent investigations. So far these studies have concentrated on total and energy-resolved ionization probabilities [1–6]. Theoretical work in this context has focused on numerical approaches [4] that often employ the sudden-impact approximation and on one-dimensional models [5,6] which try to capture the most significant physical effects occurring along the direction of polarization of a linearly polarized HCP.

In this paper a multidimensional semiclassical description of excitation of a weakly bound Rydberg electron by a half-cycle pulse is developed. It quantitatively connects the quantum evolution of the Rydberg electron to its underlying classical dynamics. The presented theoretical treatment is nonperturbative, and is applicable to arbitrary spatial and temporal HCP shapes. In particular, the approach is not restricted to the sudden-impact approximation. Within this theoretical framework measurable transition probabilities are represented as coherent sums of probability amplitudes which are associated with corresponding classical trajectories of the excited Rydberg electron. This method is very accurate numerically, especially for highly excited Rydberg states with large principal quantum numbers and for HCP's whose transferred energy is small in comparison with typical ground-state ionization energies. It is precisely this dynamical regime which usually causes severe numerical problems in fully quantum-mechanical calculations due to the large spatial extension of Rydberg states and the presence of the Coulomb singularity close to the nucleus.

On the basis of this theoretical treatment, we demonstrate that angular distributions of ionization probabilities contain a wealth of information about the ionization dynamics of the Rydberg electron which cannot be obtained from energy-resolved ionization spectra alone. In the sudden-impact approximation, for example, in which the pulse duration of the exciting HCP is small in comparison with the classical Kepler period of the Rydberg electron, energy- and angle-resolved ionization spectra are dominated by oscillatory structures and semiclassical catastrophes of the rainbow and glory types. These structures can be explained in a clear and intuitive way in terms of interferences between probability amplitudes of a few classical electronic trajectories. The study of the influence of finite-pulse durations indicates that some parts of these oscillatory structures depend strongly on the duration of the exciting HCP. A main purpose of our subsequent discussion is thus a systematic exploration of these latter effects which cannot be described appropriately by the sudden-impact approximation. First results of our studies were presented in Ref. [7].

This paper is organized as follows: In Sec. II a general (multidimensional) semiclassical description of excitation of a weakly bound Rydberg electron by a HCP is developed. This general approach is valid for arbitrary spatial and temporal dependences of the HCP. Starting from this general approach the simplifications arising in the sudden-impact ap-

proximation are discussed in detail. In Sec. III we first present a characterization of the various types of energy- and angle-resolved ionization spectra that can be obtained in the sudden-impact approximation. These spectra may be classified according to the appearing semiclassical scattering phenomena. Subsequently, it is investigated how a finite duration of the exciting HCP influences the behavior of the spectra. The comparison with the corresponding results obtained in the sudden-impact approximation demonstrate which dynamical aspects are particularly sensitive to pulse duration effects. Finally, in Sec. IV a brief summary and conclusions are given.

II. THEORETICAL DESCRIPTION

In the first part of this section a nonperturbative semiclassical framework is developed that describes the excitation of a weakly bound Rydberg electron by a HCP, and that is valid for arbitrary spatial and temporal pulse shapes. In the second part this treatment is specialized to the case of short HCP's whose influence on a Rydberg electron can be described within the sudden-impact approximation. Hartree atomic units are used with $\hbar = m_e = e = 1$ (m_e and e denote the electronic mass and charge).

A. General multidimensional semiclassical description

Let us consider a typical process in which a weakly bound Rydberg electron is excited by a half-cycle pulse. The dynamics of the electronic wave function $|\psi\rangle_t$ is described by the time-dependent Schrödinger equation $id|\psi\rangle_t/dt = H|\psi\rangle_t$, with the Hamiltonian

$$H = \tfrac{1}{2}[-i\nabla_{\mathbf{x}} - \mathbf{A}(\mathbf{x},t)]^2 + V(\mathbf{x}). \tag{1}$$

Outside the core region the effective potential $V(\mathbf{x})$ experienced by the Rydberg electron is of the form $V(\mathbf{x}) \simeq -1/|\mathbf{x}|$, whereas inside it is modified due to the presence of the other electrons and of the nucleus. The electromagnetic vector potential of the exciting HCP is denoted $\mathbf{A}(\mathbf{x},t)$ and fulfills the relations $\nabla \cdot \mathbf{A}(\mathbf{x},t) = 0$ and $\mathbf{A}(\mathbf{x}, t \to -\infty) = 0$.

Initially the Rydberg electron is supposed to be prepared in an energy eigenstate $|n_0 l_0 m_0\rangle$ with a principal quantum number $n_0 \gg 1$ and angular quantum numbers l_0 and m_0. Well inside the classically allowed region and for low values of the angular momenta, i.e. $l_0, m_0 \ll n_0$, this state can be approximated semiclassically by [8]

$$\langle \mathbf{x}|n_0 l_0 m_0\rangle = A_{\mathrm{cl}}(\mathbf{x})[e^{iS_0(\mathbf{x}) - i\pi/4} + e^{-iS_0(\mathbf{x}) + i\pi/4}], \tag{2}$$

with the classical eikonal

$$S_0(\mathbf{x}) = \int_0^{|\mathbf{x}|} dr' p(r', \epsilon_0) - (l_0 + 1/2)\pi + \pi\alpha. \tag{3}$$

The local radial electronic momentum in the Coulomb potential of the ionic core is given by

$$p(r', \epsilon_0) = \sqrt{2(\epsilon_0 + 1/r')}, \tag{4}$$

with the initial energy

$$\epsilon_0 = -[2(n_0 - \alpha)^2]^{-1}. \tag{5}$$

While the rapidly oscillating part of the wave function (2) is determined by the eikonal $S_0(\mathbf{x})$, its slowly varying amplitude is given by

$$A_{\mathrm{cl}}(\mathbf{x}) = \frac{Y_{l_0}^{m_0}(\Theta,\Phi)}{|\mathbf{x}|(n_0 - \alpha)^{3/2}\sqrt{2\pi p(|\mathbf{x}|, \epsilon_0)}}, \tag{6}$$

with the spherical harmonic $Y_{l_0}^{m_0}(\Theta,\Phi)$. The spherical angles of $\mathbf{x}$ are denoted Θ and Φ, respectively. Equation (2) is valid for electronic distances $r = |\mathbf{x}|$ from the nucleus which are located well outside the core region. All electron correlation effects are localized inside this core region, which has an extension of a few Bohr radii. They can be taken into account within the framework of quantum defect theory [9,10]. In the case of an inert ionic core which is considered here for the sake of simplicity these core effects can be described by a single quantum defect α. This quantum defect is approximately energy independent sufficiently close to the ionization threshold. Generalizations to more complicated situations in which electronic core excitations and channel couplings have to be taken into account are possible within the framework of multichannel quantum defect theory [9,10], but will not be considered in this work.

In Eq. (2) the initial state $|\psi\rangle_{t=0}$ is represented by a sum of contributions each of which involves a slowly varying amplitude, i.e., $A_{cl}(\mathbf{x})$, and an exponential function with a large, imaginary-valued argument, i.e., $iS_0(\mathbf{x})$. Within the semiclassical treatment one associates with each of these contributions a three-dimensional Lagrangian manifold in phase space [11,12]. The special form of the initial condition of Eq. (2) implies that this Lagrangian manifold has two branches, namely

$$L_0^{\pm} = \{(\mathbf{x}_0, \mathbf{p}_0) \in \mathbb{R}^6 | \mathbf{p}_0 = \pm \nabla_{\mathbf{x}_0} S_0(\mathbf{x}_0) \in \mathbb{R}^3\}. \tag{7}$$

As $S_0(\mathbf{x}_0)$ depends only on the radial electronic distance $r_0 = |\mathbf{x}_0|$ one finds $\mathbf{p}_0 = \pm |\mathbf{p}_0| \mathbf{x}_0/|\mathbf{x}_0|$ as long as $n_0 \gg l_0, m_0$. Semiclassically, the solution of the time-dependent Schrödinger equation $|\psi\rangle_t$ is determined by all solutions $\mathbf{x}_{\pm}(t; \mathbf{x}_0, \mathbf{p}_0)$ and $\mathbf{p}_{\pm}(t; \mathbf{x}_0, \mathbf{p}_0)$ of the classical equations of motion with Hamiltonian

$$H_{\mathrm{cl}} = \tfrac{1}{2}[\mathbf{p} - \mathbf{A}(\mathbf{x},t)]^2 + V(\mathbf{x}), \tag{8}$$

whose initial conditions are located in this Lagrangian manifold $L_0^{\pm}$. The probability amplitude $\langle \mathbf{x}|\psi\rangle_t$ is determined by all those classical trajectories $\{\mathbf{x}_{\pm}^{(j)}(t; \mathbf{x}_0^{(j)}, \mathbf{p}_0^{(j)}), \mathbf{p}_{\pm}^{(j)}(t; \mathbf{x}_0^{(j)}, \mathbf{p}_0^{(j)})\}$ which reach point $\mathbf{x}$ at time t, i.e. [11],

$$\langle \mathbf{x}|\psi\rangle_t = \sum_j \left(\left| \frac{dx \wedge dy \wedge dz}{dx_0 \wedge dy_0 \wedge dz_0} \right|_t^{-1/2} \right)_j \times e^{i[S_j(\mathbf{x},t) - \pi\mu_j/2]} \langle \mathbf{x}_0^{(j)}|\psi\rangle_{t=0}. \tag{9}$$

For each contributing trajectory j this probability amplitude is determined by three characteristic classical properties, namely, its classical action

$$S_j(\mathbf{x},t)=\int_0^t dt'\,\mathcal{L}(\dot{\mathbf{x}}^{(j)}(t'),\mathbf{x}^{(j)}(t'),t'), \tag{10}$$

the determinant of its Jacobi field [13]

$$\left(\left.\frac{dx\wedge dy\wedge dz}{dx_0\wedge dy_0\wedge dz_0}\right|_t\right)_j \equiv \left(\left.\mathrm{Det}\frac{\partial(x,y,z)}{\partial(x_0,y_0,z_0)}\right|_t\right)_j, \tag{11}$$

and its Morse index μ_j. Thereby, $\mathcal{L}(\dot{\mathbf{x}},\mathbf{x},t)$ denotes the classical Lagrange function associated with the Hamiltonian of Eq. (8). The determinant of the Jacobi field characterizes the stability properties of the contributing classical trajectory. The Morse index μ is numerically equal to the numbers of zeroes of this determinant times their multiplicities [13].

From Eq. (9) one can evaluate the probability amplitude of measuring an ionized electron with final momentum $\mathbf{p}^{(f)}$. With the help of the stationary phase approximation, one obtains the result

$$\begin{aligned}\langle \mathbf{p}^{(f)}|\psi\rangle_{t\to\infty} &\equiv \lim_{t\to\infty}(2\pi)^{-3/2}\int d^3\mathbf{x}\, e^{i[\epsilon^{(f)}t-\mathbf{p}^{(f)}\cdot\mathbf{x}]}\langle\mathbf{x}|\psi\rangle_t \\ &= \sum_j P_j^{(\mathrm{cl})} e^{i[S_j(\mathbf{p}^{(f)})+W_j(\mathbf{x}_0^{(j)})-i\pi\tilde{\mu}_j/2]}.\end{aligned} \tag{12}$$

This ionization amplitude is represented as a sum of all trajectories j which start at positions $\mathbf{x}_0^{(j)}$ with momenta $\mathbf{p}_0^{(j)}$ and which assume the final momentum $\mathbf{p}^{(f)}$ long after the interaction with the HCP, i.e., at $t\to\infty$. In Eq. (12) the quantity

$$P_j^{(\mathrm{cl})}=A_{\mathrm{cl}}(\mathbf{x}_0^{(j)})\left|\left(\frac{dp_x^{(f)}\wedge dp_y^{(f)}\wedge dp_z^{(f)}}{dx_0\wedge dy_0\wedge dz_0}\right)_j^{-1/2}\right| \tag{13}$$

denotes the classical contribution of trajectory j to the angle- and energy-resolved ionization probability. The classical action $S_j(\mathbf{p})$ is given by

$$S_j(\mathbf{p})=-\int_0^\infty dt\,\mathbf{x}^{(j)}(t)\cdot\frac{d\mathbf{p}^{(j)}(t)}{dt}-\mathbf{x}^{(j)}(t=0)\cdot\mathbf{p}^{(j)}(t=0).$$

The phase contribution originating from the initial state is determined by

$$W_j(\mathbf{x})=\pm[S_0(\mathbf{x})-\pi/4], \tag{14}$$

where one has to choose the plus or minus sign depending on whether the initial radial momentum of the Rydberg electron is positive or negative. The Maslov index $\tilde{\mu}_j$ is equal to the number of zeroes of the determinant $(dp_x^{(f)}\wedge dp_y^{(f)}\wedge dp_z^{(f)}/dx_0\wedge dy_0\wedge dz_0)_j$ times their multiplicities [11]. In terms of the ionization amplitude of Eq. (12) the energy- and angle-resolved ionization probability is given by

$$\frac{dP_{\mathrm{ion}}}{d\epsilon^{(f)}d\Omega}=\sqrt{2\epsilon^{(f)}}|\langle\mathbf{p}^{(f)}|\psi\rangle_{t\to\infty}|^2 \tag{15}$$

with $d\Omega=\sin\Theta_f d\Theta_f d\Phi_f$, and with Θ_f and Φ_f denoting the spherical angles of the final momentum $\mathbf{p}^{(f)}$.

Equations (12) and (15) are main results of this section. They yield a complete and numerically accurate (compare with Sec. III A) semiclassical description of the influence of an arbitrary HCP on a weakly bound Rydberg electron that is prepared initially in an energy eigenstate. These equations are based on Maslov's multidimensional generalization of the Jeffreys, Wentzel, Kramers, and Brillouin (JWKB) method as applied to the time-dependent Hamiltonian of Eq. (1) [11]. It should be mentioned that there exists also a wealth of alternative semiclassical methods to approach initial value problems. These methods have been pioneered by Heller [14] and Miller [15], and have been generalized recently in various directions [16–18]. These types of semiclassical approximations are mainly based on the dynamics of Gaussian wave packets [19], and so far they have been applied predominantly to problems with explicit time-independent Hamiltonians.

If the initial state of the Rydberg electron is not an energy eigenstate of the form of Eq. (2), almost all of the considerations of this section still apply. It is only the classical Lagrangian manifold associated with the initial state that has to be modified appropriately. In the case of a spatially localized electronic Rydberg wave packet, for example, which can be described by a quantum state of the form

$$\langle\mathbf{x}|\psi\rangle_{t=0}=B(\mathbf{x})e^{iR(\mathbf{x})}, \tag{16}$$

with a large eikonal $R(\mathbf{x})$ and a slowly varying amplitude $B(\mathbf{x})$ the associated Lagrangian manifold is given by

$$L_0=\{(\mathbf{x}_0,\mathbf{p}_0)\in\mathbb{R}^6|\mathbf{p}_0=\nabla_{\mathbf{x}_0}R(\mathbf{x}_0)\in\mathbb{R}^3\}. \tag{17}$$

Contrary to the initial state considered in Eq. (2) this Lagrangian manifold has only one branch, so that the structure of the interferences appearing in Eq. (12) is expected to be changed significantly.

Finally, we would like to mention a useful scaling property of the classical Hamiltonian (8). If spatial variations of the pulses are negligible the classical trajectories $(\mathbf{x}(t),\mathbf{p}(t))$ and $(\tilde{\mathbf{x}}(t),\tilde{\mathbf{p}}(t))$ induced by two HCP's $\mathbf{A}(t)$ and $\tilde{\mathbf{A}}(t)=\gamma\mathbf{A}(\gamma^3 t)$ are related by the scaling relations

$$\begin{aligned}\tilde{\mathbf{x}}(t)&=\gamma^{-2}\mathbf{x}(\gamma^3 t),\\ \tilde{\mathbf{p}}(t)&=\gamma\mathbf{p}(\gamma^3 t).\end{aligned} \tag{18}$$

These scaling properties are exploited in Sec. III A, where they simplify the classification of the types of spectra obtainable in the sudden-ionization approximation.

B. Semiclassical treatment in the sudden-impact approximation

If the pulse duration τ of the exciting HCP is small in comparison with the classical Kepler period $T_{\mathrm{cl}}=2\pi(n_0-\alpha)^3$ of the initially prepared Rydberg electron, the determination of $|\psi\rangle_t$ can be simplified considerably. Neglecting

for the sake of clarity any spatial dependence the vector potential of the applied HCP can be approximated by

$$\mathbf{A}(t) = -\Theta(t)\Delta\mathbf{p}, \tag{19}$$

with the characteristic momentum

$$\Delta\mathbf{p} = -\int_{-\infty}^{\infty} dt\, \mathbf{E}(t). \tag{20}$$

Thereby, $\mathbf{E}(t) = -d\mathbf{A}/dt$ denotes the HCP field strength. Thus the solution $|\psi\rangle_t$ of the time-dependent Schrödinger equation with Hamiltonian (1) is approximately given by

$$|\psi\rangle_t = e^{-iH_A t} e^{i\Delta\mathbf{p}\cdot\hat{\mathbf{x}}} |\psi\rangle_{t=0} \quad (t>0), \tag{21}$$

with the atomic Hamiltonian $H_A = \frac{1}{2}(-i\nabla_{\mathbf{x}})^2 + V(\mathbf{x})$. Within this sudden-impact approximation, the Rydberg electron experiences a sudden change of its momentum by the amount $\Delta\mathbf{p}$ and subsequently evolves under the influence of the atomic Hamiltonian H_A without being further affected by the HCP. In this case ionization probabilities can also be evaluated quantum mechanically by means of a partial wave analysis.

In the case of a hydrogen atom, for example, which is prepared initially in the state $|n_0, l_0 = m_0 = 0\rangle$ the angle- and energy-resolved ionization probability is given by the partial-wave expansion

$$\frac{dP_{\text{ion}}}{d\epsilon^{(f)}\, d\Omega} = \frac{1}{\sqrt{2}\pi |\mathbf{p}^{(f)}|} \sum_{l=0}^{\infty} e^{i\sigma_l} P_l(\cos\Theta_f) \times \int_0^{\infty} dr\, S_{n_0, l_0=0}(r) j_l(|\Delta\mathbf{p}| r) F_l(\epsilon^{(f)}; r). \tag{22}$$

Thereby P_l and j_l are the Legendre polynomial and the spherical Bessel function of order l, respectively. The regular, energy-normalized radial Coulomb wave function is denoted $F_l(\epsilon^{(f)}; r)$, and σ_l is the Coulomb phase shift. The radial wave function of the initially prepared Rydberg state $|n_0, l_0 = m_0 = 0\rangle$ is denoted $S_{n_0, l_0=0}$. In Eq. (22) it has been assumed that the HCP is linearly polarized, and that the spherical angles (Θ_f, Φ_f) of the final momentum $\mathbf{p}^{(f)}$ are measured with respect to the direction of polarization.

Alternatively, $|\psi\rangle_t$ can also be determined semiclassically with the approach developed in Sec. II A. For this purpose one starts from the electronic state which is modified by the sudden momentum change due to the HCP. Immediately after the application of the HCP, this state is given by

$$|\psi\rangle_{t=+0} = e^{i\Delta\mathbf{p}\cdot\hat{\mathbf{x}}} |\psi\rangle_{t=-0}. \tag{23}$$

If the Rydberg electron is prepared initially in the energy eigenstate $|\psi\rangle_{t=-0} = |n_0 l_0 m_0\rangle$ of Eq. (2), the classical Lagrangian manifold which is associated with this state is given by

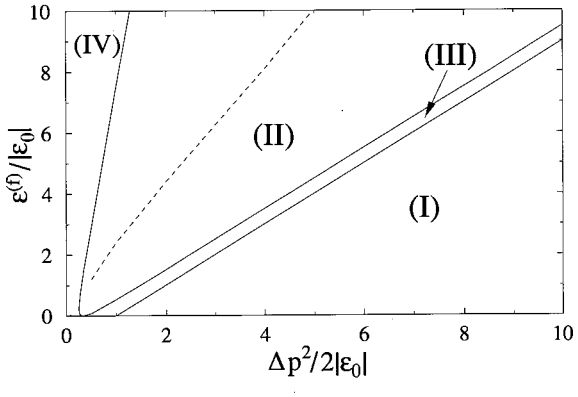

FIG. 1. Classification of ionization spectra in the sudden-impact approximation. The following semiclassical catastrophes are observed in the respective areas of the plane spanned by $\Delta p^2/2|\epsilon_0|$ and $\epsilon^{(f)}/|\epsilon_0|$: (*I*) forward and backward glory; (*II*) rainbow and backward glory; (*III*) two rainbows, and forward and backward glory; and (*IV*) no semiclassical catastrophes. For a given value of $\Delta p^2/2|\epsilon_0|$ the ionization probability $dP_{\text{ion}}/d\epsilon^{(f)}$ is concentrated below the dashed line [in the sense that $dP_{\text{ion}}/d\epsilon^{(f)} < 0.025(dP_{\text{ion}}/d\epsilon^{(f)})_{\max}$, approximately, beyond this line].

$$L_0^{\pm} = \{(\mathbf{x}_0, \mathbf{p}_0) \in \mathbb{R}^6 | \mathbf{p}_0 = \pm\nabla_{\mathbf{x}_0} S_0(\mathbf{x}_0) + \Delta\mathbf{p} \in \mathbb{R}^3\}. \tag{24}$$

In analogy to Eq. (9), the probability amplitude $\langle\mathbf{x}|\psi\rangle_t$ is determined by all solutions of the classical equations of motion with Hamiltonian

$$H_{A,\text{cl}} = \frac{\mathbf{p}^2}{2} + V(\mathbf{x}), \tag{25}$$

whose initial conditions are located in this Lagrangian manifold. As this Hamiltonian is explicitly time independent, the energy of these trajectories is conserved during their time evolution. This implies that outside the core region where $V(\mathbf{x}) \approx -1/|\mathbf{x}|$ the initial positions $\mathbf{x}_0$ on this Lagrangian manifold which yield ionizing trajectories with final energy $\epsilon^{(f)}$ are determined by energy conservation, i.e.,

$$\frac{1}{2}[\pm\nabla_{\mathbf{x}_0} S_0(\mathbf{x}_0) + \Delta\mathbf{p}]^2 - \frac{1}{|\mathbf{x}_0|} = \epsilon^{(f)}. \tag{26}$$

Inserting Eq. (3) and assuming a linearly polarized HCP with $\Delta\mathbf{p} = \Delta p\, \mathbf{e}_z$, $\Delta p > 0$, yields

$$\frac{1}{|\mathbf{x}_0|} = \frac{(\epsilon^{(f)} - \epsilon_0 - \Delta p^2/2)^2}{2\Delta p^2 \cos^2\Theta_0} - \epsilon_0, \tag{27}$$

with Θ_0 denoting the polar angle of the initial position $\mathbf{x}_0$. Equation (27) determines the initial positions $\mathbf{x}_0$ of the classical trajectories which ionize with asymptotic energy $\epsilon^{(f)}$. According to Eq. (27), there is one value of $r_0 = |\mathbf{x}_0|$ for each final energy $\epsilon^{(f)}$ and initial angle Θ_0. At the critical final energy $\epsilon_{\text{crit}}^{(f)} = \epsilon_0 + \Delta p^2/2$ the local radial momentum of Eq. (4) vanishes, and the primitive semiclassical approximation for the initial state $|n_0 l_0 m_0\rangle$ is no longer applicable. In this special case a proper semiclassical description of the initial state can be obtained with the help of uniform semiclassical

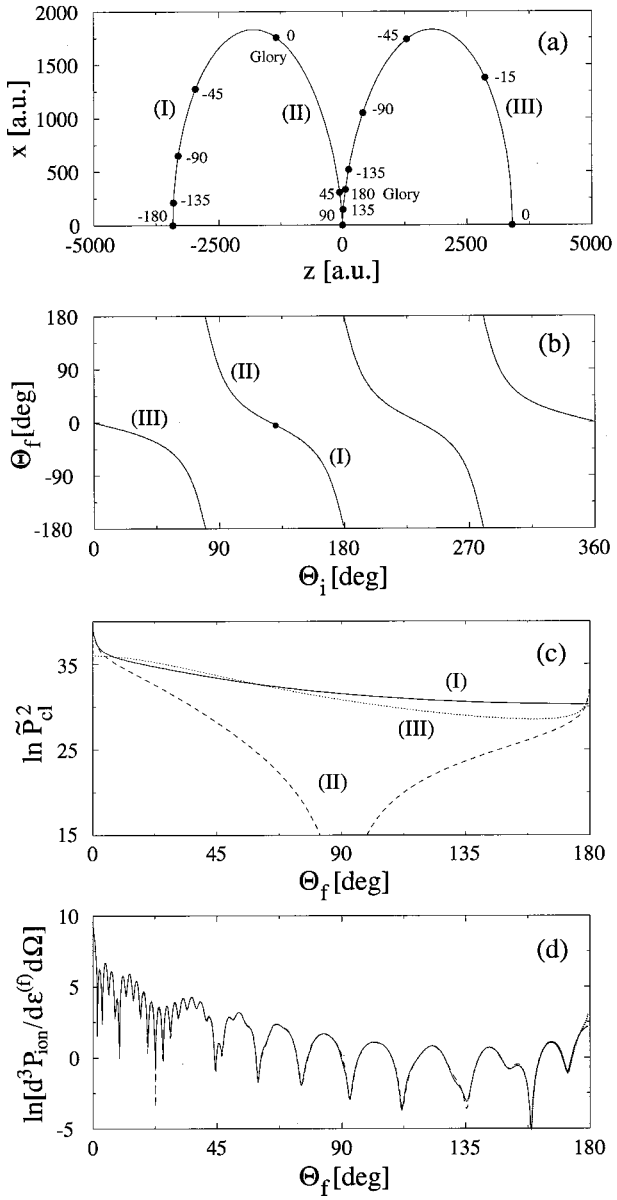

FIG. 2. (a) Initial positions of classical trajectories with $\Delta p^2/2|\epsilon_0|=6.25$, $\epsilon^{(f)}/|\epsilon_0|=1.84$, and $n_0=50$ according to Eq. (27). The numbers indicate final emission angles Θ_f for specific initial positions. Angles are counted counterclockwise from the z axis. The figure has to be continued into three dimensions by rotation around the z axis. The roman numbers relate the different trajectory classes to diagram (c). Axes are labeled in atomic units. (b) Final angle Θ_f as a function of the polar angle Θ_i of the corresponding initial position. (c) Classical weight $\tilde{P}^2_{\rm cl}=|P_{\rm cl}|^2/|A_{\rm cl}(\mathbf{x}_0)|^2$ (in a.u.) as a function of Θ_f for the trajectory classes distinguished in (a). (d) Angular distribution of the ionized electron $\ln\{d^3P_{\rm ion}/d\epsilon^{(f)}\,d\Omega[\text{a.u.}]\}$ in the sudden-impact approximation: quantum-mechanical (full), uniform semiclassical (dashed), and primitive semiclassical (dotted) results.

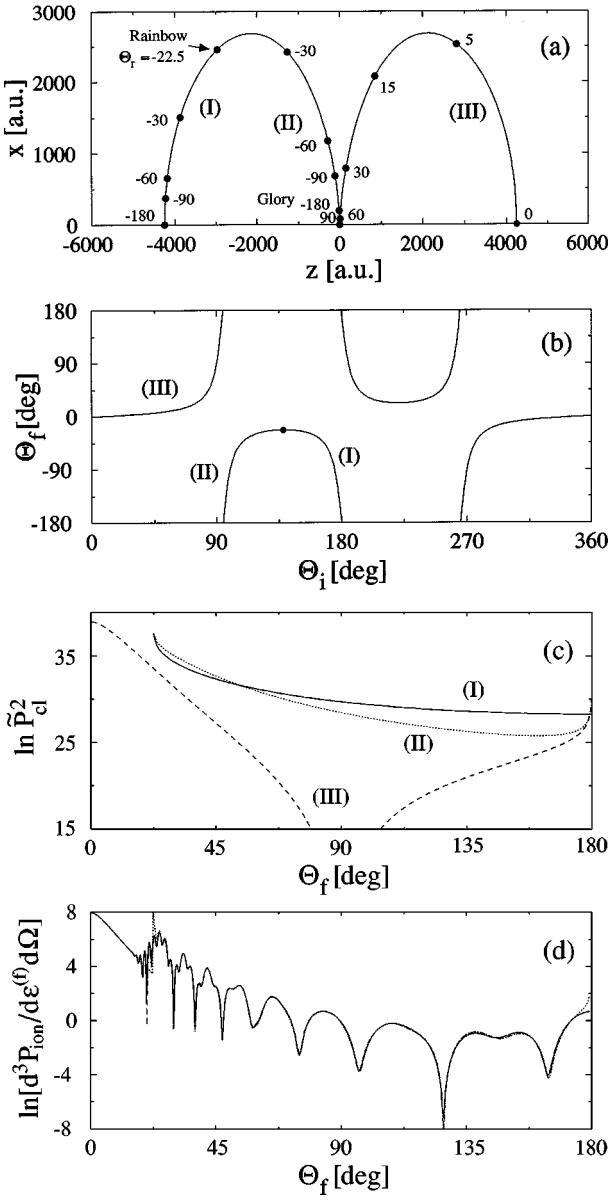

FIG. 3. Same as Fig. 2 for $\epsilon^{(f)}/|\epsilon_0|=7.35$.

methods [20]. This peculiar property suggests that one can at least distinguish two different energy regimes in the excitation of a Rydberg electron by a HCP, namely, a region of low final energies for which $\epsilon^{(f)}<\epsilon^{(f)}_{\rm crit}$ and a high-energy regime in which $\epsilon^{(f)}>\epsilon^{(f)}_{\rm crit}$. For a fixed value of the final ionization energy $\epsilon^{(f)}$, the initial positions of the classical trajectories which ionize into a particular final angle Θ_f have to be determined by the solutions of the classical equations of motion with Hamiltonian (25). In the special case of a hydrogen atom these relations can be evaluated analytically [21]. A comprehensive discussion of energy- and angle-resolved ionization probabilities which is based on the semiclassical results of this section is presented in Sec. III.

III. ENERGY- AND ANGLE-RESOLVED IONIZATION SPECTRA

In this section energy- and angle-resolved ionization probabilities are discussed on the basis of the semiclassical approach developed in Sec. II. In the first part, characteristic predictions of the sudden-impact approximation are discussed in the semiclassical limit. The second part discusses modifications of these ionization spectra that arise from a finite duration of the exciting HCP.

A. Sudden-impact approximation

This part gives a general overview of the characteristic properties of angle- and energy-resolved ionization spectra in the sudden-impact approximation for the case $l_0, m_0 \ll n_0$. As will be shown below, these spectra can be described very accurately with the help of semiclassical methods. Thus the characteristic qualitative aspects of their behavior may be understood by studying the underlying classical dynamics.

The classical trajectories pertaining to the parameter sets $(\epsilon_0, \Delta p, \epsilon^{(f)})$ and $(\gamma^2\epsilon_0, \gamma\Delta p, \gamma^2\epsilon^{(f)})$, $\gamma > 0$, are related by the scaling transformation of Eq. (18). Therefore, it is sufficient to examine the classical dynamics as a function of the parameters $\Delta p^2/2|\epsilon_0|$ and $\epsilon^{(f)}/|\epsilon_0|$, for example. The result of a corresponding study is summarized in Fig. 1. In this diagram various regions in the $(\Delta p^2/2|\epsilon_0|, \epsilon^{(f)}/|\epsilon_0|)$ plane are identified that give rise to different types of behavior of the ionization spectra.

Region (I) pertains to parameters with $0 < \epsilon^{(f)} < \epsilon^{(f)}_{\rm crit} \equiv \Delta p^2/2 + \epsilon_0$. According to Eq. (27), in this case classical trajectories start with negative (positive) radial momenta $-(+)\nabla_{\mathbf{x}_0} S_0(\mathbf{x}_0)$ from the positive (negative) z half-plane. In order to illustrate the typical behavior of the resulting spectra we consider as an example the parameter values $\Delta p^2/2|\epsilon_0| = 6.25$, $\epsilon^{(f)}/|\epsilon_0| = 1.84$. Figure 2(a) depicts the initial positions of the classical trajectories in the (x,z) plane, and their respective final angles for the initial principal quantum number $n_0 = 50$ (which implies $\epsilon^{(f)} = 10\,\text{meV}$). To show the distribution of the scattering angles clearly, in Fig. 2(b) the ''deflection function'' is displayed, i.e., the dependence of the final angle Θ_f on the polar angle Θ_i of the corresponding initial position. From Figs. 2(a) and 2(b) it is apparent that three different initial positions pertain to each final emission angle Θ_f. The relative significance of these trajectory classes for the ionization signal can be inferred from Fig. 2(c), where their classical weights $\tilde{P}^2_{\rm cl} = |P_{\rm cl}|^2/|A_{\rm cl}(\mathbf{x}_0)|^2$ (i.e., the Jacobi determinants) are depicted as a function of the final angle Θ_f. For small and very large final angles the contributions of all three classes are relevant whereas in the intermediate region the weight of class (II) becomes negligibly small. This decrease is due to the fact that class (II) includes trajectories with initial positions $\mathbf{x}_0$ in the vicinity of $\mathbf{x} = \mathbf{0}$, and the behavior of such trajectories depends very sensitively on the initial conditions. As shown in Fig. 2(d), the existence of different contributing trajectories with approximately equal weight leads to pronounced interference effects in the ionization spectrum. In particular, for small angles, one observes rapid oscillations which gradually diminish as Θ_f is increased. This diminution is directly related to the peculiar Θ_f-dependence of the classical weight of trajectory class (II) that was described above.

An important feature of Figs. 2(a) and 2(b) is the existence of trajectories with $\Theta_f = 0°$ (180°), whose initial positions do not lie on the z axis. Consequently, due to the rotational symmetry of the system around this axis, there are infinitely many classical trajectories that contribute to the ionization amplitude at these final angles so that the classical probabilities $|P_{\rm cl}|^2$ diverge there. This phenomenon is known as semiclassical glory scattering [20]. For a proper semiclassical description the primitive ionization amplitude of Eq. (12) has to be regularized with the help of uniformization methods [20]. Thereby, one replaces the contributions of the trajectory classes a and b at both sides of the divergence by the uniform expression

$$e^{i[(f_a+f_b)/2-\tilde{\mu}_b\pi/2-\pi/4]}\sqrt{\frac{\pi(f_a-f_b)}{4}}\{(g_a+g_b)J_0[(f_a-f_b)/2]+i(g_a-g_b)J_1[(f_a-f_b)/2]\}, \tag{28}$$

with $f_j = S_j + W_j(\mathbf{x}_0^{(j)})$ and $g_j = P_j^{(\rm cl)}$ $(j = a,b)$. The trajectories are labeled in such a way that $f_a > f_b$ so that $\tilde{\mu}_a = \tilde{\mu}_b + 1$. The Bessel functions of order zero and one are denoted $J_0(x)$ and $J_1(x)$. The contribution of the third trajectory can be described by the primitive semiclassical expression given in Eq. (12). In Fig. 2(d) the quantum-mechanical ionization spectrum (full curve) is compared to the uniform (dashed) and the primitive (dotted) semiclassical approximation. All spectra in this section are calculated for an initial hydrogenic energy eigenstate with $l_0 = 0$. The uniform curve describes the quantum-mechanical result very well over the whole angular range whereas the primitive approximation diverges in small regions around $\Theta_f = 0°$ and 180°. The characteristic qualitative features of the example described above, i.e., the existence of three contributing trajectories for all angles $0° < \Theta_f < 180°$, their relative weights and the appearance of forward and backward glory effects are characteristic for all spectra represented by region (I) of Fig. 1.

The second region of particular importance in Fig. 1 is denoted (II). This region is bounded from below and above by the curves

$$E^2 + 2(1-3\Delta)E + 8\Delta\sqrt{E\Delta} - 3\Delta^2 - 2\Delta + 1 = 0 \tag{29}$$

and

$$E^2 + 2(1-3\Delta)E - 8\Delta\sqrt{E\Delta} - 3\Delta^2 - 2\Delta + 1 = 0, \tag{30}$$

with $E = \epsilon^{(f)}/|\epsilon_0|$ and $\Delta = \Delta p^2/2|\epsilon_0|$ [22]. For $\Delta \gg 1$, relations (29) and (30) can be approximated as $E = \Delta - 1/2$ and $E = 9\Delta - 3/2$, respectively. The spectra in region (II) are characterized by the appearance of a semiclassical rainbow scattering phenomenon and a backward glory whereas the forward glory present in the spectra of region (I) has disappeared. Again, this behavior is most clearly illustrated by studying a particular example. To this end, the parameter values $\Delta p^2/2|\epsilon_0| = 6.25$, $\epsilon^{(f)}/|\epsilon_0| = 7.35$ are used (with n_0

$=50$ in Fig. 3, which implies $\epsilon^{(f)}=40\,\mathrm{meV}$). In contrast to the previous case (and, more generally, as soon as $\epsilon^{(f)}>\epsilon_0+\Delta p^2/2$) trajectories originating from the positive (negative) z half-plane now start with positive (negative) radial momentum. Figure 3(a) depicts the location of initial positions in the (x,z) plane and their corresponding final angles, whereas Fig. 3(b) again shows the deflection function. Apparently, for final angles larger than the ''rainbow angle'' Θ_r the contributions of three different trajectory classes have to be taken into account. At Θ_r, however, two of these classes coalesce which gives rise to the semiclassical rainbow scattering phenomenon [20]. Again the classical weights of the corresponding classical trajectories diverge at this angle [cf. Fig. 3(c)]. To determine the transition amplitude the primitive approximation has to be replaced by a uniformized expression. Using the notation of expression (28) and defining $\xi=[3(f_1-f_2)/4]^{2/3}$, this uniform transition amplitude takes the form

$$\sqrt{\pi}e^{i[(f_1+f_2)/2-\tilde{\mu}_2\pi/2-\pi/4]}\{(g_1+g_2)\xi^{1/4}\mathrm{Ai}(-\xi)+i(g_1-g_2)\xi^{-1/4}\mathrm{Ai}'(-\xi)\}. \tag{31}$$

In Eq. (31), $\mathrm{Ai}(\xi)$ and $\mathrm{Ai}'(\xi)$ denote the Airy function and its derivative. Quantum mechanically, the rainbow scattering phenomenon does not cease abruptly at the rainbow angle, but extends smoothly into the classically forbidden region. This may be taken into account semiclassically by extrapolating the quantities f_i, g_i, and ξ of expression (31) to values $\Theta_f<\Theta_r$.

Furthermore, Figs. 3(a)–3(c) show that the forward glory has disappeared but that the backward glory is still present. The classical weight associated with the different types of trajectories can be inferred from Fig. 3(c). Figure 3(d) shows that the most prominent difference between the spectra of cases (I) and (II) is that the latter start for small angles with a smooth nonoscillating part. Oscillations set in only around Θ_r.

If, for a fixed value of $\Delta p^2/2|\epsilon_0|$, the final energy $\epsilon^{(f)}/|\epsilon_0|$ is increased, the rainbow angle Θ_r grows toward a value of 180°, and the interference effects in the spectrum are more and more diminished. If the line given by Eq. (30) is crossed, rainbow and backward glory scattering vanish completely. In this region (IV), the spectrum is determined by the contributions of a single trajectory class, and interferences are no longer visible. However, Fig. 1 also indicates that in this dynamical region the angle-integrated ionization probability $dP_{\mathrm{ion}}/d\epsilon^{(f)}$ is very small, so that this type of behavior is only of little practical relevance, in general.

Regions (I) and (II) are separated by a small area (III) in which the classical dynamics is more complicated. In this transition region besides the backward glory both forward glory and rainbow scattering characteristic of regions (I) and (II) are present. In addition, however, a second classical rainbow angle appears at a very small value of Θ_f. A proper semiclassical description of this behavior would require uniformization based on a higher-order catastrophe [20].

Figures 2(a) and 3(a) indicate that there is a strong correlation between the final direction into which the electron is emitted and its position before application of the pulse. This correlation might be useful for probing the spatial distribution of localized wave packets. In order to assess the perspectives of such an approach, in Fig. 4 we plot several ionization spectra obtained in the sudden-impact approximation. They pertain to a radial Rydberg wave packet detected at different stages of its time evolution. For the calculation, the wave packet was assumed to be generated by a weak and short laser pulse as described in Ref. [23], and the electronic angular momentum was taken as $l_0=0$ to show the effects in question most clearly. The spectral envelope $\tilde{\mathcal{E}}(\epsilon)$ of the laser pulse was chosen as $\tilde{\mathcal{E}}(\epsilon)\propto\exp[-(\epsilon-\overline{\epsilon})^2(\delta t)^2]$ with the mean excited energy $\overline{\epsilon}=-2\times10^{-4}$ a.u. corresponding to a

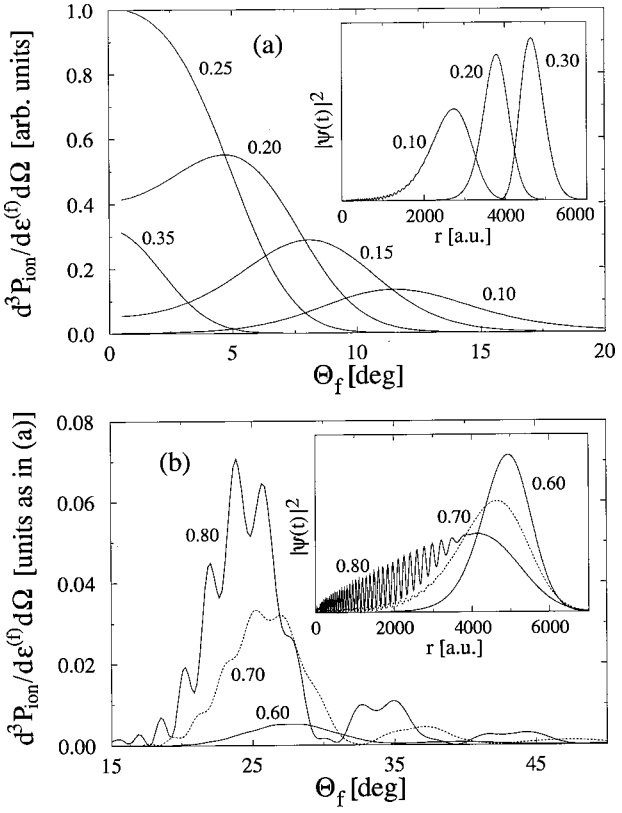

FIG. 4. Angle- and energy-resolved ionization spectra obtained from radial Rydberg wave packets in the sudden-impact approximation. (a) Outward-traveling wave packets; the respective delay times between excitation and probing are indicated in units of the classical wave packet orbit time $T_{\mathrm{cl}}=20\,\mathrm{ps}$. (b) Incoming wave packets. Radial distributions of the wave packet at different times are shown in the insets. All relevant parameter values are given in the text.

mean quantum number $\bar{n}=50$ and an energy spread determined by $\delta t=0.035T_{\rm cl}$. Figure 4(a) shows the spectra (on a nonlogarithmic scale) for $\epsilon^{(f)}=40$ meV and various delay times between the exciting laser pulse and the HCP with $\Delta p=0.05$ a.u. All delay times are chosen such that the wave packet has not yet reached its outer turning point and is still moving outward. The inset depicts some corresponding radial distributions $|\psi(t)|^2$ for the wave packet. The connection between these distributions and the form of the spectra can be made with the help of the right part of Fig. 3(a), where $z>0$. As long as $|\psi(t)|^2$ is peaked at a distance r_c less than ~ 4000 a.u., the spectrum attains its maximum at an angle $\Theta_f>0$ whose value agrees with what can be inferred directly from r_c and Fig. 3(a). For larger values of r_c the maximum is reached at $\Theta_f=0°$, but decreases as the wave packet moves beyond 4000 a.u.

For the case of an inward-moving wave packet, which is examined in Fig. 4(b), the spectra are essentially peaked around the rainbow angle Θ_r independent of the delay time. This observation agrees again with the classical picture obtained from Fig. 3 as the associated weight of the electron trajectories diverges at this angle. In order to achieve a connection between the maxima in the spectrum and the electronic probability distribution similar to Fig. 4(a), one should investigate spectra for final energies $\epsilon^{(f)}<\epsilon^{(f)}_{\rm crit}$ [cf. Fig. 2(a)]. In summary, Fig. 4 demonstrates that the spatial distribution of the wave packet is indeed reflected in the ionization spectrum. In order to obtain a complete picture of the distribution, one will have to analyze a set of spectra with different parameters. A particular advantage of the use of HCP's, compared, e.g., to optical methods, is that they can interact with the wave packet at every point of its orbit.

B. Finite-duration HCP's

In this subsection we discuss to what extent the results of Sec. III A can be applied to the study of angle- and energy-resolved ionization spectra from HCP's of finite duration. It is natural to examine this problem within a semiclassical approach as the theoretical framework discussed in Sec. II can be applied equally well to both instantaneous and time-dependent pulses, and its quantitative accuracy has been demonstrated in Sec. III A. Thus the main task consists of studying the classical electronic dynamics. In a fully quantum-mechanical treatment, the partial-wave expansion of Sec. II B would no longer be applicable. One would have to turn to a numerical integration of the time-dependent Schrödinger equation which is significantly more complicated due to the Coulomb singularity at the nucleus, and due to the large spatial extension of highly excited Rydberg states.

In the present context our main question is to which extent the essential results of the sudden-impact approximation can be recovered in experiments with finite-duration HCP's. It is therefore reasonable to concentrate the study on short pulses with durations τ up to the order of, say, one-tenth of the Rydberg electron's orbit time $T_{\rm cl}$. Typically this corresponds to pulse lengths around 1 ps which can easily be produced in the laboratory. Before discussing in detail an example that illustrates characteristic effects originating from

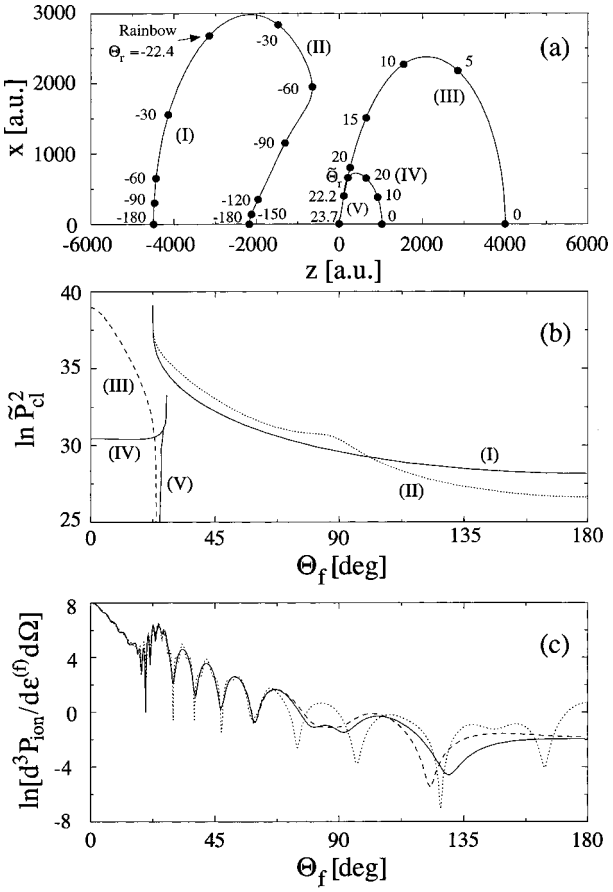

FIG. 5. Same as Fig. 3 but now for the quasirectangular HCP of duration $T_p=0.05T_{\rm orb}$ described in the text (deflection function not shown). (a) The new trajectory classes which are denoted (IV) and (V) are separated by the ''rainbow point'' $\tilde{\Theta}_r$. The initial points for (V) almost coincide with those for (III) (but the initial radial momenta are opposite). Indicated angles refer to (III). (c) Full curve: ionization probability for the pulse described above. Dashed: sine-shaped pulse as described in the text. Dotted: result of the sudden-impact approximation.

finite-duration HCP's, let us briefly summarize the main results of our investigations.

(i) The behavior of trajectories starting close to the nucleus is modified significantly even by very short pulses, whereas the dynamics of orbits originating at a large distance from the core is changed only very gradually. This is of course due to the different initial velocities of the trajectories: far away from the nucleus, the electron moves slowly, and the pulse can still be considered as almost instantaneous. From Figs. 2 and 3, it follows that the part of the spectrum with small final angles Θ_f, where the ionization probability is concentrated and where forward glory and rainbow scattering can be observed, is related to trajectories with large initial distances from the nucleus. Thus these essential regions of the spectrum can be expected to be relatively insensitive to effects of finite-pulse durations. On the other hand, the behavior of the spectrum at large final angles is determined by trajectories starting close to the core. In this region of the spectrum, where the ionization probability is relatively small, pulse duration effects are most prominent. In particular, in our examples we even find backward glory scattering to vanish.

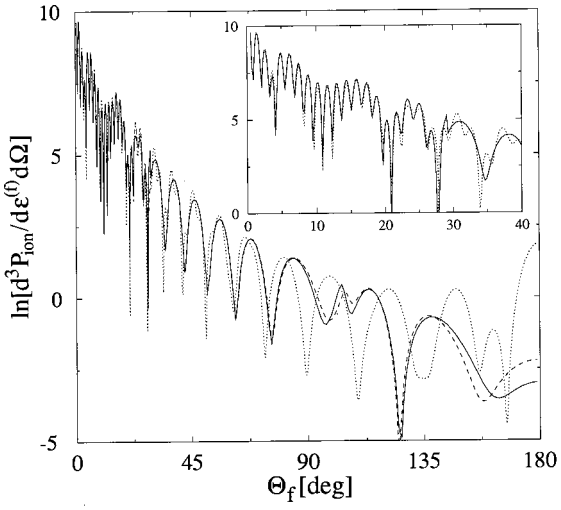

FIG. 6. Same as Fig. 5(c) for $\epsilon^{(f)}/|\epsilon_0|=3.68$. The inset shows the spectra for the quasirectangular pulse described in the text (full curve), and for the sudden-impact approximation (dotted curve) at small angles.

(ii) The deviations of the spectrum from the sudden-impact approximation are mainly determined by the pulse duration, whereas details of the pulse shape seem to be of less importance. We compared the classical dynamics and spectra resulting from two types of HCP's, the shapes of which were almost rectangular and a half-period sine wave, respectively. These choices should represent typical variations of realistic HCP shapes. The differences in the resulting spectra for these two pulse forms (calculated for identical pulse durations and integrated field strengths) were small in comparison to the deviations from the sudden-impact approximation [see Figs. 5(c) and 6].

(iii) In the sudden-impact approximation there are classical trajectories for *all* values of final energies $0<\epsilon^{(f)}<\infty$. With increasing pulse duration, however, we find that the range of accessible final energies becomes more and more reduced in accordance with the energy-time uncertainty principle mentioned in Sec. I.

In order to discuss effects of finite-pulse duration in more detail, we consider as an example the ionization spectrum for an HCP with an almost rectangular pulse shape given by $\mathbf{E}(t)=\mathbf{e}_z E_0 \exp[-(t/t_0)^8]$. The parameters E_0 and t_0 are determined so that the integrated field strength and the pulse duration fulfill $\Delta p^2/2|\epsilon_0|=6.25$ and $\tau/T_{\rm cl}=0.05$, respectively. Again, for the calculation an initial hydrogenic energy eigenstate with $l_0=0$ and with a principal quantum number $n_0=50$ was chosen. Figure 5 shows an analysis of the corresponding classical dynamics and of the resulting ionization spectrum for a final energy of $\epsilon^{(f)}/|\epsilon_0|=7.35$ (compare to Fig. 3). Figure 5(a) details the changes in the classical dynamics. Three major modifications can be observed.

(a) The final angles Θ_f of trajectories with initially outgoing radial momentum do not cover the full range $0°<\Theta_f<90°$ as in the sudden-impact approximation. Instead, they are restricted to values $0<\Theta_f<\Theta_m$ with $\Theta_m\approx 23.7°$ in the present case. Here this does not lead to major changes in the spectrum. This is because in the angular region where the deviations of this trajectory class from the sudden-impact case become significant the dominant contributions already originate from trajectory classes (*I*) and (*II*) [see Figs. 3(b) and 5(b)]. However, due to the absence of trajectory class (*III*) for $\Theta_f>\Theta_m$ the small short-period modulations of the spectrum of Fig. 3(c), which are visible for Θ_f between 25° and 55°, are no longer present in Fig. 5(c).

(b) A new class of trajectories appears which has no counterpart in the sudden-impact approximation. These orbits have initially incoming radial momenta and originate from the half-plane $z>0$. Their final angles vary between 0° and 27.5°. The maximum final angle is not attained at ($x=0$, $z=0$), but at a finite distance from the nucleus so that there is a rainbow effect connected with this class of trajectories [cf. Fig. 5(b)]. However, due to the low classical weight of these trajectories, they show up in the spectrum most prominently in the form of small modulations in the vicinity of $\Theta_f=0°$.

(c) The initial positions of trajectories which start with incoming radial momenta from the half-plane $z<0$ are changed significantly. In addition, the final angle $\Theta_f=180°$ is reached only for initial positions with $z=0$, so that backward glory scattering has disappeared. The changes in the ionization spectrum at large angles which are due to these effects represent the most significant influence of finite pulse durations.

In Fig. 5(c) the resulting ionization spectrum (full curve) is compared to a spectrum which has been calculated for a HCP of identical integrated field strength and pulse duration but with shape $\mathbf{E}(t)=\mathbf{e}_z E_0' \sin(2\pi t/\tau')$, $t\leq\tau'/2$ (dashed curve). The spectrum for the sudden-impact approximation is also shown (dotted curve). As mentioned above, for these pulse durations the influence of the HCP shape is only secondary even for large final angles. However, as the pulse length is increased to values larger than $\sim 0.1T_{\rm orb}$, these influences eventually become more significant. Figure 6 shows the results of an investigation similar to Fig. 5(c) for a final energy of $\epsilon^{(f)}/|\epsilon_0|=3.68$ ($\epsilon^{(f)}=20$ meV) which corresponds to region (*I*) of the sudden-impact approximation (cf. Fig. 1). As in the previous case, it is found that the main features of the spectrum of the sudden-impact approximation are left almost unchanged. The classical dynamics change similarly to the previous example. In particular, the new trajectory class still exists, but in the rapidly oscillating part of the spectrum its contribution is almost undiscernible.

IV. SUMMARY AND CONCLUSIONS

A general semiclassical treatment of excitation of weakly bound Rydberg electrons by intense HCP's has been presented. Thus a quantitative connection between observable transition probabilities and the underlying classical dynamics of the excited Rydberg electron has been established. This approach is numerically accurate for high principal quantum numbers of the Rydberg electron, and in cases in which the energy transfer from the exciting HCP to the Rydberg electron is small in comparison with typical ionization energies of low-lying states. The underlying classical dynamics of the Rydberg electron yields a clear and natural explanation for the oscillatory structures which govern the resulting energy- and angle-resolved ionization spectra. These structures arise from interference between probability amplitudes associated with different ionizing trajectories. Thereby two types of semiclassical catastrophes appear, namely, glory scattering

for electron emission in the forward and backward direction of the polarization of the HCP and a rainbow phenomenon. Parts of these oscillatory structures depend strongly on the ratio between the pulse duration of the exciting HCP and the classical Kepler period of the initially prepared Rydberg state. The amplitude and phase information which is contained in the semiclassical probability amplitudes might be useful for the reconstruction of quantum states of Rydberg electrons. A first indication of the usefulness of such an approach was given by the investigation of the spectra pertaining to radial wave packets.

ACKNOWLEDGMENTS

G.A. acknowledges support by the Deutsche Forschungsgemeinschaft within the SPP ''Zeitabhängige Phänomene und Methoden.'' O.Z. was supported by the U.S. Office of Naval Research under Contract No. 14-91-J1205, and by the U.S. Army Research Office.

[1] R. R. Jones, D. You, and P. H. Bucksbaum, Phys. Rev. Lett. **70**, 1236 (1993); N. E. Tielking and R. R. Jones, Phys. Rev. A **52**, 1371 (1995); R. B. Vrijen, G. M. Lankhuijzen, and L. D. Noordam, Phys. Rev. Lett. **79**, 617 (1997).
[2] R. R. Jones, Phys. Rev. Lett. **76**, 3927 (1996).
[3] C. Raman *et al.*, Phys. Rev. Lett. **76**, 2436 (1996).
[4] C. O. Reinhold, H. Shaw, and J. Burgdörfer, J. Phys. B **27**, L469 (1994); K. J. La Gattuta and P. B. Lerner, Phys. Rev. A **49**, R1547 (1994); A. Bugacov *et al.*, Phys. Rev. A **51**, 1490 (1995); C. O. Reinhold *et al.*, J. Phys. B **28**, L457 (1995); C. O. Reinhold *et al.*, Phys. Rev. A **54**, R33 (1996); M. T. Frey *et al.*, *ibid.* **55**, R865 (1997); R. Gebarowski, J. Phys. B **30**, 2143 (1997); S. Yoshida *et al.*, Phys. Rev. A **58**, 2229 (1998).
[5] M. Mallalieu and Shih-I Chu, Chem. Phys. Lett. **258**, 37 (1996).
[6] C. D. Schwieters and J. B. Delos, Phys. Rev. A **51**, 1023 (1995); **51**, 1030 (1995).
[7] G. Alber and O. Zobay, Phys. Rev. A **59**, R3174 (1999).
[8] H. A. Bethe and E. Salpeter, *Quantum Mechanics of One- and Two-Electron Atoms* (Plenum, New York, 1977).
[9] M. J. Seaton, Rep. Prog. Phys. **46**, 167 (1983).
[10] U. Fano and A. R. P. Rau, *Atomic Collision and Spectra* (Academic, New York, 1986).
[11] V. P. Maslov and M. V. Fedoriuk, *Semiclassical Approximation in Quantum Mechanics* (Reidel, Boston, 1981).
[12] J. B. Delos, Adv. Chem. Phys. **65**, 161 (1986).
[13] L. S. Schulman, *Techniques and Applications of Path Integration* (Wiley, New York, 1981).
[14] E. J. Heller, J. Chem. Phys. **75**, 2923 (1981).
[15] W. H. Miller, Adv. Chem. Phys. **25**, 69 (1974).
[16] M. F. Herman and E. Kluk, Chem. Phys. **91**, 27 (1984).
[17] K. G. Kay, J. Chem. Phys. **100**, 4377 (1994).
[18] G. Campolieti and P. Brumer, Phys. Rev. A **50**, 997 (1994).
[19] F. Grossmann, Comments At. Mol. Phys. **34**, 141 (1999).
[20] M. V. Berry and K. E. Mount, Rep. Prog. Phys. **35**, 315 (1972).
[21] L. D. Landau and E. M. Lifshitz, *Mechanics* (Pergamon, Oxford, 1976).
[22] Relations (29) and (30) can be derived by noting that $\partial\Theta_f/\partial x_0(z_0=0)|_{\epsilon^{(f)}=\text{const}}$ changes sign when the boundary between regions (*II*) and (*III*) [or (*IV*), respectively] is crossed.
[23] G. Alber, H. Ritsch, and P. Zoller, Phys. Rev. A **34**, 1058 (1986).